Comprehensive Radial Filter Design for Practical higher-order Ambisonic Recording

Stefan Lösler[1], Franz Zotter[2]
[2]*Institut für Elektronische Musik und Akustik*
[1,2]*Kunstuniversität Graz, Austria, Email: stefanloesler@gmail.com*

Introduction

There are several microphones on the market for recordings in B-format, but only a few for higher-order Ambisonic such as the *mhacoustics Eigenmike EM32* which can be seen in Fig. 1. To enable Ambisonic surround playback, its microphone signals are first transformed into spherical-harmonics-domain signals by a frequency-independent matrix. Such signals are not directly applicable for playback. Roughly speaking, this is because low-frequency signals predominantly map to a non-directional (zeroth-order) pattern on the surface of the microphone array, so that higher-order signals require amplification. Therefore, the transformation is followed by holographic (radial) filters that yield the B-format signals needed for higher-order Ambisonic playback [2] [3].

Figure 1: mh acoustics' *Eigenmike* EM32 microphone for 4$^{\text{th}}$ order Ambisonic recording.

Theoretical radial filtering applies extremely large bass boosts for high orders, where, in addition to a correct treatment of the signal, they amplify self-noise and sensitivity differences between the microphones by a disastrous amount. Practical radial filtering must be limited to a maximum amplification, e.g., by Tikhonov filters of Moreau [3], or soft-limiting by Bernschütz [4].

Rettberg [5] shows the white noise gain (WNG) as a result of amplification limitation of radial filters. In fact WNG should be taken into account to define the crossover frequencies instead of any dB-level limits.

How a phase-matched soft limiting can be realized based on classical filter design methods is presented by Baumgartner [6]. However, all-pass filters for phase matching could only be approximated, and we found the later IIR implementation to be numerically critical.

Barely did the above-presented soft-limiting filters consider (1) equalization, i.e. compensation for amplitude losses due to the omitted high-order signals, (2) adaptation of order weights (e.g. max-rE [1]) to all frequency bands for an optimal suppression of all directional side lobes, or (3) that limiting filters together with radial filters should have a slope of about min. +6dB/oct to similarly suppress low-frequent noise in signals of all orders.

To improve all-pass matching in soft-limiting by classical filters, Linkwitz-Riley high- and low-pass pairs are used, for which an identical-phase all pass exists. The graphical description used in [9] was found to improve the presentation of the final time-frequency-direction behavior.

This contribution describes how such a band-pass filter bank can be designed to include all desired features.

The filterbank

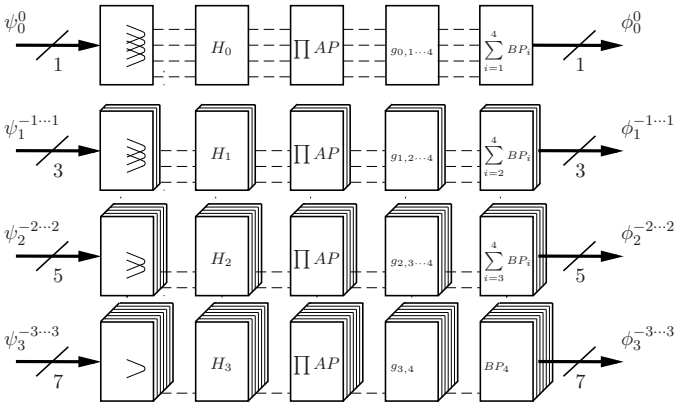

Figure 2: Structure of the filter bank, with band-pass filter, radial filter, all-pass filter, order and frequency band weighting.

Fig. 2 shows the structure of the proposed filter bank. The Ambisonic signal is split up in band-pass channels, whose number depends on the maximum Ambisonic order. Band splitting is followed by corresponding radial filters and all-pass phase equalization. All passes model what is missing from phase responses of the other band-pass channels and yield a fully phase-identical sub-band decomposition. Hereby the filter bank is amplitude-complementary and always free from destructive interference, as long as the filter bank weights stay positive. A detailed view of a single Ambisonic signal is shown in Fig. 3.

Radial filters

The signals ψ_{nm} are the spherical wave spectrum representing the spherical-harmonic encoded sound pressure p on the spherical microphone array. They are found by the above-mentioned frequency-independent matrixing of $\boldsymbol{p}$, the array signals, $\boldsymbol{\psi} = \boldsymbol{E}\,\boldsymbol{p}$. From ψ_{nm}, the Ambisonic B-format signals are obtained by holographic radial filters

$$\phi_{nm} = kR^2\,\frac{h_n'(kR)}{h_n(kr_s)}\,\psi_{nm} \qquad (1)$$

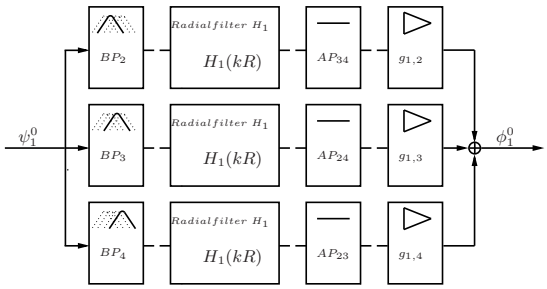

Figure 3: Single filter channel for the Ambisonic signal ψ_1^0 from Fig. 2.

that determine the Ambisonic signals on a desired playback radius r_s. Filters depend on the array radius R and the wave number k. h_n are the Hankel functions and h_n' their derivatives [10][6].

We assume that the sources lie in the farfield, $r_s \to \infty$, for which the Hankel functions approach

$$\lim_{r_s \to \infty} h_n(kr_s) = \frac{\mathrm{i}^{(n+1)} e^{-\mathrm{i}kr_s}}{kr_s}, \qquad (2)$$

and hereby simplify the radial filters (constant factors r_s and R^2 can be cancelled)

$$\phi_{nm} = r_s (kR)^2 \, h_n'(kR) \, e^{ikr_s} (-\mathrm{i})^{n+1} \, \psi_{nm}. \qquad (3)$$

Because of the far-field approximation, the saturation of the filters at lower frequencies is missing and they get even more unstable. Nevertheless, the far-field approximation beneficially shifts all critical poles to $s = 0$, which unifies the stabilization we intend to undertake. Fig. 4 compares far-/near-field radial filtering for a source radius $r_s = 3\mathrm{m}$.

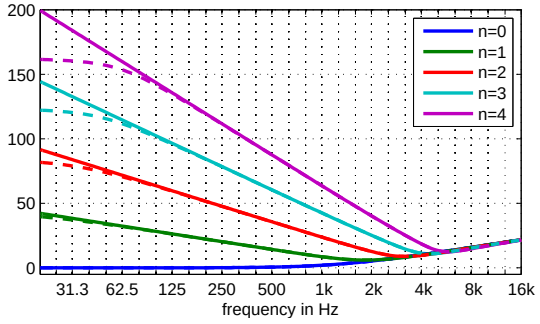

Figure 4: Far-field approximation of radial filters for the *Eigenmike* compared to near-field filters (dashed) for $r_s = 3\mathrm{m}$.

After transferring the filters from the Laplace s- to the z-domain [6], we observe the multiple poles from $s = 0$ at $z = 1$, Fig. 5. We are going to cancel these poles by a high-pass filter design to provide an efficient and stable implementation. To suppress low frequency noise by at least a +6dB high-pass skirt, high pass filters are designed to contain at least one more zero at $z = 1$ than Eq. (3).

Exact phase match: Linkwitz-Riley filters

For each radial filter of a specific order, a high-pass filter is used to soft-limit its dynamics at a suitable cut-on frequency.

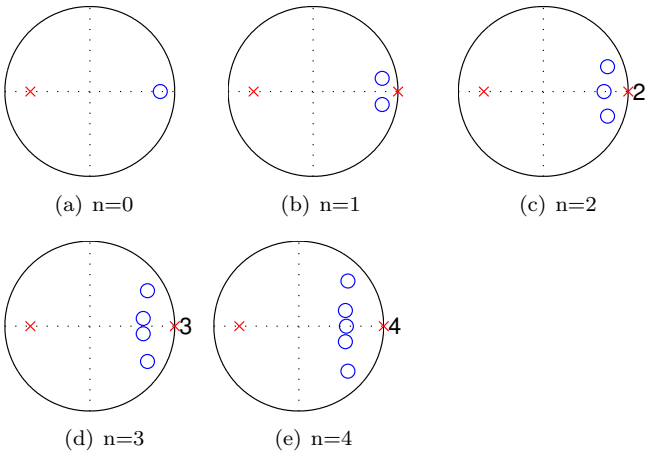

Figure 5: Poles-(red cross)- and zeros-(blue circle) distribution of the radial filters in the z-domain for the *Eigenmike*.

To allow different treatment of the ramaining lower-order signals below this frequency, they are split into a high-pass and low-pass band by a crossover at this frequency.

Not only is an accurately phase-matching crossover required to avoid destructive interference when recombining the two differently weighted lower-order bands, but also the high pass that soft-limits the respective high-order signals must phase-match the crossover to retain a useful surround point-spread function near the cut-on frequency.

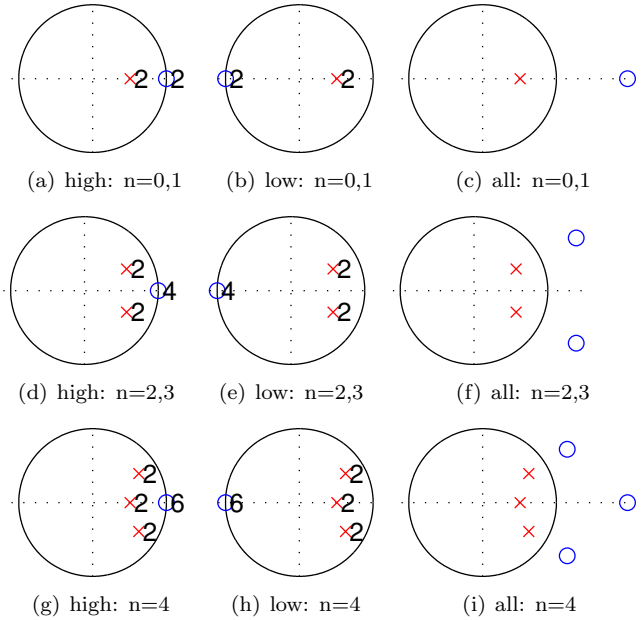

Figure 6: Pole-zero plots of 2^{nd}, 4^{th}, and 6^{th} order discrete-time Linkwitz-Riley crossovers transformed to $\pi/5$, exemplarily. High- and low-pass (left, middle) are exactly amplitude-complementary and phase-identical with the all-pass (right).

In the master thesis [12], perfectly phase-matching, amplitude-complementary crossovers were proposed employing Linkwitz-Riley [8] filter pairs.

To preserve the phase match when splitting into more than 2 bands, we can employ suitable Linkwitz-Riley all-passes to obtain an accurately phase-matched filterbank with all the soft-limiting cut-on frequencies.

Table 1: Number of zeros for the high-pass filter to roll of radial filter at least by 6 dB/oct.

n	no. poles RF	req. no. zeros	closest L-R order
0	0	1	2
1	1	2	2
2	2	3	4
3	3	4	4
4	4	5	6

Linkwitz-Riley filters are of even order, as they are built from the square of Butterworth filters [13]. To operate the filters in discrete time, the bilinear transform yields their z-domain representation. Fig. 6 shows the zero and pole positions 2^{nd}, 4^{th}, and 6^{th} order Linkwitz-Riley filters.

The filterbank is composed of Linkwitz-Riley, high-, low-, and all-passes of the cutoff frequencies f_b, such that

$$B_b(\omega) = H_{f_{b-1}}(\omega)\, L_{f_b}(\omega) \prod_{b' \setminus \{b-1,b\}} A_{f_b}(\omega). \qquad (4)$$

After including the radial filter in the band-pass filter bank, their poles cancel with zeros from the corresponding high-pass filter; to obtain a stable implementation, canceling poles have to be explicitly removed. The resulting frequency response is adjusted to yield a 1^{st} or 2^{nd} high-pass skirt to guarantee a roll-off of noisy signals towards the low frequency end. Table 1 shows the number of poles and zeros of the implementation.

Order weights and frequency band weights

Directional side lobe suppression (order weights)

The max-r_E order weighting [1] suppresses directional side lobes in the surround *point-spread function* that maps a recorded plane wave. The filter-bank design allows to weight of every frequency band $b = 0 \ldots 4$, individual to its maximum order $N = b$.

The max-r_E weights [7] are non-zero for $n \leq b$

$$\begin{aligned} g_{nb} &= a_{nb}/\epsilon_b, \qquad (5) \\ a_{nb} &= P_n\Big(\cos\Big(\frac{137.9^\circ}{b+1.51}\Big)\Big), \end{aligned}$$

where P_n is the Legendre polynomial and ϵ_b is the equalization defined in the next paragraph.

Equalization (frequency band weights)

The weights $1/\epsilon_b$ in Eq. (5) ensure equalization of the frequency bands by either the amplitude of the omnidirectional component, of the free field (on-axis response), or of the diffuse field (random directional energy efficiency):

$$\epsilon_b = \begin{cases} 1, & \text{omni-dir. amplitude,} \\ \sqrt{\sum_{n=0}^{b} a_{nb}^2 (2n+1)}, & \text{diffuse-field amplitude,} \\ \sum_{n=0}^{b} a_{nb}(2n+1), & \text{free-field amplitude.} \end{cases} \qquad (6)$$

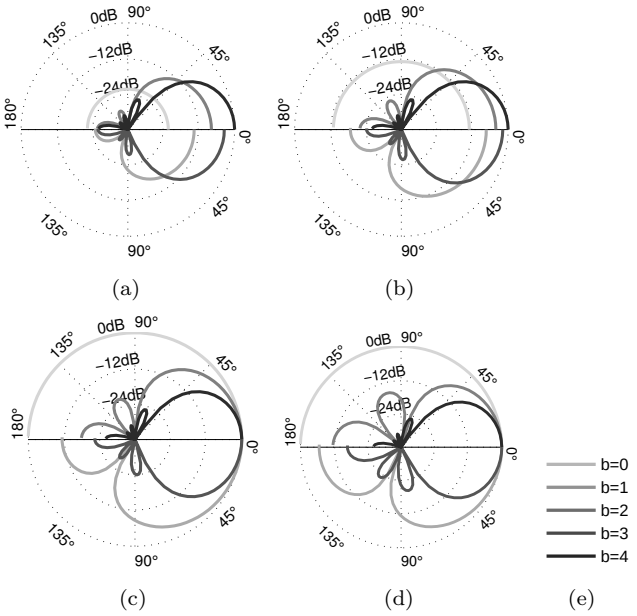

Figure 7: Frequency-band-specific point-spread functions mapping a recorded plane-wave. Curves are (a) without, (b) with diffuse-field, or (c) with free-field equalization across 5 bands of increasing order $N = b$, see (e); odd orders are plotted on lower semicircle for good readability [(d) non-individual max-rE weights $b < 4$ lack side-lobe suppression.]

Ideal patterns across the frequency bands are shown in Fig. 7. Note that diffuse- and free-field equalization require gains of 13 and 22 dB in the lowest frequency band.

Cut-on frequencies that limit noise-boost

To limit the maximum noise amplification within the entire set of Ambisonic signals, the cut-on/cross-over frequencies of the filter bank must be carefully adjusted. The adjustment is accomplished by the non-linear minimization of the cut-on frequencies using lsqnonlin (MATLAB) under the constraint of a limited white noise gain (WNG). The noise boost should stay below 20 dB. In total, the low self noise (15 dBA) of each of the 32 microphones slightly decreases (13 dBA) by matrixing to 25 spherical-harmonic signals, and it is finally boosted by the subsequent 20dB-WNG-limited radial filters (33 dBA).

The noise boost $G(\omega)$ is proportional to

$$|G(\omega)|^2 \propto \sum_{b=0}^{4} \sum_{n=0}^{b} (2n+1) \left| g_{bn} B_b(\omega) \cdot (kR)^2 h_n'(kR) \right|^2, \qquad (7)$$

and the optimizer finds the lowest-possible cut-on frequencies f_b defining the band-passes $B_b(\omega)$ achieving the limited noise boost $|G(\omega)| < 20$ dB, see Tab. 2.

Table 2: Frequencies of filterbank providing a 20 dB-limited noise boost (lowest cut-on was manually defined).

b	$f_b^{\text{no-eq}}$	f_b^{diffuse}	f_b^{free}
0	20 Hz	20 Hz	20 Hz
1	68 Hz	59 Hz	140 Hz
2	478 Hz	612 Hz	800 Hz
3	1405 Hz	1534 Hz	1702 Hz
4	2727 Hz	2742 Hz	2766 Hz

Point spread in time, frequency, direction

Of a recorded sound, the proposed implementation variants yield a point-spread across time, frequency, and direction, cf. Fig. 8. The plots display the magnitude of the point spread as brightness and its phase in color.

The proposed design (shown for $\phi > 0$) exhibits group delay distortion but minimal pre-ringing in time (right col.). An alternative zero-phase representation of the filterbank (shown for $\phi < 0$) yields identical beam patterns in the frequency domain (left col.) but pre-ringing in time.

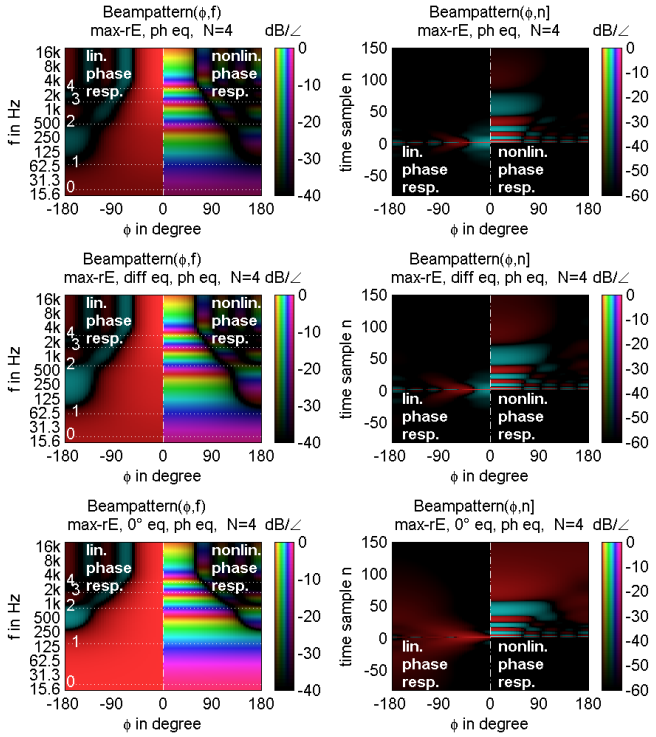

Figure 8: Point-spread functions [9] in frequency (left) and time (right) over different directions for order N=4, comparing the zero-phase ($\phi < 0$) and non-linear phase implementations ($\phi > 0$); omnidirectional equalization (top row), diffuse-field equalization (middle row), free-field equalization (bottom row).

Conclusion

We presented a soft-knee limiting filter bank for radial filtering in higher-order Ambisonic recordings, based on Linkwitz-Riley filter pairs, which allowed us to design nonlinear-phase IIR and comparable linear-phase FIR filter banks yielding identical beam patterns. Most importatly, our design approach limits radial filters towards low frequencies to prevent low-frequency noise, allows to control directional side lobes, and provides equalization.

The phase responses of all involved filter bands match exactly, also far from the crossovers by additional all pass filtering. The accurate phase match prevents cancellations between differently-weighted filter bank channels and preserves meaningful surround point-spread functions.

The proposed design is implemented and successfully in use for demonstrations and music pieces at IEM that use Ambisonic microphohe and spherical loudspeaker arrays.

Future work should study the following perceptual questions: *Which equalization is the best for Ambisonics: omni-directional, diffuse-field, or free-field? How should the filters be implemented, non-linear phase or zero phase?* Listening tests should be done to evaluate.

References

[1] J. Daniel, J.-B. Rault, and J.-D. Polack, "Ambisonics Encoding of Other Audio Formats for Multiple Listening Conditions," in *Audio Engineering Society Convention 105*, Sept. 1998.

[2] J. Daniel and S. Moreau, "Further study of sound field coding with higher order ambisonics," in *Audio Engineering Society Convention 116*, May 2004.

[3] S. Moreau, "Etude et realisation d'outils avances d'encodage spatial pour la technique de spatialisation sonore higher order ambisonics : microphone 3d et controle de distance," PhD Thesis, Academie de Nantes, Le Mans, France, 2006.

[4] B. Bernschütz, C. Pörschmann, S. Spors, and S. Weinzierl, "Soft-limiting der modalen amplitudenverstärkung bei sphärischen mikrofonarrays im plane wave decomposition verfahren," in *Proc. of the 37. Jahrestagung für Akustik (DAGA)*, 2011.

[5] T. Rettberg and S. Spors, "On the impact of noise introduced by spherical beamforming techniques on data-based binaural synthesis," in *Proc. of the 39. Jahrestagung für Akustik (DAGA)*, 2013.

[6] R. Baumgartner, H. Pomberger, and M. Frank, "Practical implementation of radial filters for ambisonic recordings," *ISCA*, 2011.

[7] F. Zotter and M. Frank, "All-round ambisonic panning and decoding," *J. Audio Eng. Soc*, vol. 60, no. 10, 2012.

[8] S. P. Lipshitz and J. Vanderkooy, "In-Phase Crossover Network Design," *J. Audio Eng. Soc*, vol. 34, no. 11, 1986.

[9] T. Rettberg and S. Spors, "Time-domain behaviour of spherical microphone arrays at high orders," in *Proc. of the 40. Jahrestagung für Akustik (DAGA)*, 2014.

[10] F. Zotter, "Analysis and synthesis of sound-radiation with spherical arrays," PhD Thesis, Institut für Elektronische Musik und Akustik, Kunstuni Graz, Graz, A, 2009.

[11] E. G. Williams, *Fourier Acoustics*. Academic Press, 1999.

[12] S. Lösler, "MIMO-Rekursivfilter für Kugelarrays," Master-Thesis, Institut für Elektronische Musik und Akustik, Kunstuniverität Graz, Graz, A, 2014.

[13] U. Tietze and C. Schenk, *Halbleiter-Schaltungstechnik*. Springer, 2002.